Analysis of deformation-induced surface morphologies in steel sheet

M.R. Stoudt *, J.B. Hubbard

Materials Science and Engineering Laboratory, National Institute of Standards and Technology, 100 Bureau Drive, Stop 8553, Gaithersburg, MD 20899-8553, United States

Abstract

The surfaces of strained mild steel sheet specimens were examined with scanning laser confocal microscopy. Rigorous assessments were employed to establish the form of the roughness data. The small deviations from the ideal conditions observed in these assessments indicated that the stochastic process responsible for surface roughening does not conform to stationary, Gaussian, Markov statistics. As physical considerations make violations of the stationary and Markov properties unlikely, it was concluded that even small discrepancies in the Gaussian fit have substantial influences on the quality of roughening behavior characterizations. This also confirms that deformation-induced surface roughness occurs by a small number of statistically dominant mechanisms. Analyses of the mean amplitude (R_q) and spatial distributions both exhibited sharp changes in behavior at approximately 4% strain. Since the physical meanings of the two analyses are independent, it was concluded that this common behavior correlated with a change in dominant roughening mechanism.
Published by Elsevier Ltd on behalf of Acta Materialia Inc.

1. Introduction

Inhomogeneous surface deformation (e.g., orange-peel, banding, or roping) is a significant obstacle impeding the widespread use of the many alloys intended to increase automobile fuel economy. In addition to being cosmetically unacceptable, these surface markings have a profound detrimental affect on the formability: They localize strain, promoting component failure from tearing or wrinkling, and they alter the friction between the metal sheet and the die surfaces during metal forming [1,2]. As the surface roughening behavior essentially establishes the suitability of an individual alloy for a particular application, numeric predictions of the evolution of surface roughness have become more central in the automotive development process. At present, there are significant discrepancies between the surface morphology predicted by numeric methods and what is actually measured on the surface of real materials. These discrepancies suggest that the available surface roughness data are not adequate for the modeling requirements and that a better understanding of the measurement issues associated with the roughening process is necessary to increase the accuracy of the formability predictions.

Reports in the literature indicate that the roughening behavior of a free surface follows a relationship where the surface roughness is proportional to the amount of plastic strain [3–7]. There is also a consensus that this relationship holds regardless of the influence the material crystal structure may have on the deformation [8,9]. In contrast, plastic deformation in a polycrystalline alloy is an extremely complex process [10–12]. The roughness that occurs at a free surface strongly depends upon both the grain size [13–15] and orientation effects in the sheet [16–18], as well as upon the rate at which the deformation occurs [19,20]. These inconsistencies raise many questions about the validity of this simple

* Corresponding author. Tel.: +1 301 975 6025; fax: +1 301 975 4553.
  E-mail address: stoudt@nist.gov (M.R. Stoudt).

empirical relationship, and any prediction of the overall roughening behavior upon which it is based.

The literature clearly establishes that the accuracy of any roughness evaluation is dependent on the technique used for data acquisition and that all surface measurement methods introduce errors of some form into the data [5,21]. Radhakrishnan [22] showed how an improper ratio between the size of the measurement probe and the scale of the measured features would introduce substantial errors by masking or filtering the subtleties in the roughness profile. The characteristics of these errors are well known and appropriate measures for their correction have been established [5].

The methods used to interpret roughness data are an error source of greater significance. Most assessments of roughening behavior in the literature are derived from linear profiles (i.e., individual measurements of the surface taken in one dimension). In such an assessment, the profile is postulated to be a characteristic of the entire surface [23]. Most of the literature accounts express the roughness of the entire surface through an estimation of the mean of the amplitude distribution. The most common method is the arithmetic mean, or the R_a parameter [21]:

$$R_a = \frac{1}{L} \int_0^L |z(x)| \, dx. \tag{1}$$

In this equation, L is the length over which the profile is evaluated and $z(x)$ is the magnitude of the profile height at any point along the evaluation length. The mean amplitude distribution can also be expressed through another parameter, R_q, which is based on the root mean squared (rms). The rms roughness is expressed as:

$$R_q = \sqrt{\frac{1}{L} \int_0^L z^2(x) \, dx}. \tag{2}$$

Both of these parameters are used routinely in industrial applications to quantify the changes in surface morphology, and they are often used interchangeably even though they have different physical meanings [24]. While R_a tends to be slightly more common, it is not directly based on any statistical treatment. Conversely, R_q is defined as the standard deviation of all the heights contained in the profile. For this reason, it is regarded as a more functional representation of the mean of the amplitude distribution.

As shown by Eqs. (1) and (2), both parameters collapse an entire roughness profile into a single value. This compresses complex surface information into an expression that can be rather coarse with respect to the length scale of the surface details involved [14]. Extrapolation of this compressed value to a representation of an entire surface could introduce substantial error, as the results are highly dependent upon the statistical methods used for the analysis. Because these are average values, is it also possible for distinctly different surface morphologies to produce the same roughness value. Fig. 1 is a recent observation of such behavior [25]. Clearly, any prediction of the roughening behavior that is based solely on a mean roughness parameter is likely to be misleading. While the overall objective is a robust prediction of the mechanical behavior for any alloy under a given set of forming conditions, this particular effort evaluates the changes in roughening behavior with plastic strain for a mild steel sheet. It also examines the underlying principles used to interpret a typical surface roughness measurement.

2. Experimental procedure

Most of the surface roughness data reported in the literature are derived from measurements performed
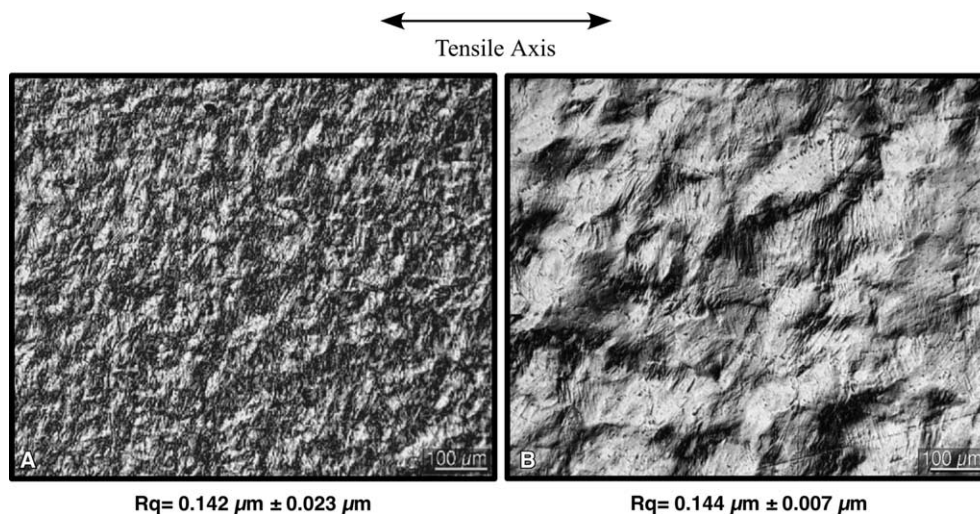
Fig. 1. Two heat treatments of an aluminum alloy exhibiting the same mean roughness values with distinctly different surface morphologies and frictional behaviors.

on samples with polished gauge sections. While polished surfaces tend to produce more consistent surface roughness measurements, the surfaces of the steel sheets used in industry are not pristine. In fact, automotive manufacturers customarily specify a maximum acceptable initial surface roughness for the metal sheet that is dependent upon the specific application (e.g., $R_a \leqslant 0.5$ μm for an outer hood panel). Therefore, all of the data in this analysis were acquired from steel sheet in the as-received condition to be more representative of actual forming conditions.

2.1. Material

Cold-rolled AISI 1010 steel sheet with a nominal 1.0 mm thickness was selected for this analysis because it is a generic alloy that demonstrates good formability, and the deformation behavior has been well established in the literature [26,27]. The 1.0 mm sheet thickness is used routinely in automotive applications. The grain size and rolling direction of the AISI 1010 steel were verified through a series of microstructural examinations. Specimens were mounted and polished according to standard metallographic procedure [28] for these studies. The final step of mechanical polishing was 0.05 μm colloidal silica after which the samples were immersed in solutions of 4-volume fraction picral and 2-volume fraction nital to reveal the microstructure.

2.2. Generation of surface roughness

Flat sheet, tensile specimens were punched from sheet stock with the tensile axis perpendicular to the rolling direction of the sheet. The critical dimensions were measured for all samples. Fiducial lines were lightly engraved at the extremes of the gauge section of each specimen with a silicon carbide scribe to facilitate a more accurate assessment of the plastic strain. The spacing between grid lines was determined with a linear-encoded, measuring stage microscope that had a resolution of ±500 nm. The specimens were pulled in uniaxial tension to pre-determined levels of plastic strain with a computer-controlled universal tensile machine that continuously monitored the applied stress and the total strain. The crosshead displacement rate was 1.0 mm/s for all of these experiments. When the desired strain level was attained, the specimen was removed from the grips, and the fiducial lines were re-measured with the microscope to assess the actual amount of plastic strain in the gauge area of the specimen.

2.3. Surface roughness measurements

The changes in the surface topographies were quantified by examining the specimen surfaces in both the as received and in the strained conditions with scanning laser confocal microscopy (SLCM). The optics of the SLCM used for this study were designed to optimize the imaging conditions for opaque materials by operating exclusively in a reflective imaging mode. More information on SLCM imaging and the surface roughness measurement methodology can be found in [29,30]. All of the SLCM images in this analysis were created with a 635 nm laser source, a 10× objective lens and a typical z-scan depth of approximately 20 μm.

These parameters generated a 640×512 pixel intensity image of the surface with both outstanding optical depth of field and spatial resolution. The corresponding (x, y, z) dimensions of the images were 1000 μm × 800 μm × 20 μm, respectively, and the spacing between the individual focal planes within each image was approximately 100 nm. Topographic maps were generated from the intensity images with the controlling software. A series of linear roughness profiles with a typical length of 750 μm were collected from the topographic maps. Each roughness profile was corrected for flatness and long wavelength effects resulting from specimen tilt or other mechanical influences. This "leveling" was accomplished with a routine in the controlling software that first calculated the best multiple regression equation for the plane from which the topographic image was acquired and then subtracted the individual points in the profile from the regression equation. The controlling software also interpolated the profile data by a factor of five. This produced a roughness profile that contained a minimum of 2400 data points and an approximate sampling interval of 300 nm. A roughness measurement consisted of five, well separated and randomly placed profiles in the parallel orientation followed by five profiles in perpendicular orientation with respect to the rolling direction of the sheet.

3. Results and discussion

3.1. Microstructure

The as received microstructure of the 1010 steel sheet was determined to consist of relatively equiaxed ferrite grains, approximately 10 μm in diameter (Table 1), and pearlite colonies. The volume fraction of pearlite (determined using ASTM E562 [31]) was found to be 0.039 ± 0.001. Other than the pearlite, the microstructure was

Table 1
Ferrite grain characteristics determined using ASTM E112 (24)

Viewing plane	Mean grain diameter (μm)	ASTM grain size
Perpendicular to normal direction	9.9 ± 1.3	10.4
Perpendicular to rolling direction	8.4 ± 0.6	10.9
Perpendicular to transverse direction	8.6 ± 0.7	10.8

completely consistent with other observations reported in the literature [32].

3.2. Analyses of height distributions

The roughness measurement data were acquired from the SLCM topography images. Fig. 2 shows a typical SLCM surface topography of the 1010 steel sheet in the as-received condition. The plot directly beneath is the surface profile of the trace shown in the upper figure. As noted previously, the mean of the amplitude distribution of a roughness profile can be expressed through either the R_a or the R_q value. The R_q parameter was selected to represent the mean of the amplitude distribution for this evaluation.

In general, the differences in behavior between the parallel and perpendicular orientations to the rolling direction of the sheet were relatively small. However, the magnitudes of the changes in the amplitudes for the perpendicular orientation were consistently larger than those observed for the parallel orientation. Fig. 3 shows the changes in surface roughness of the as-received surfaces as a function of measured strain in both the parallel and the perpendicular orientations to the rolling direction of the sheet. Unlike a polished surface where the mechanical action removes the deformed layer produced by cold rolling and minimizes the variability in surface hardness, the initial surface condition for this study was the as-received condition. Accordingly, the initial surface roughness was non-zero and all of the roughness data include the localized inhomogeneities
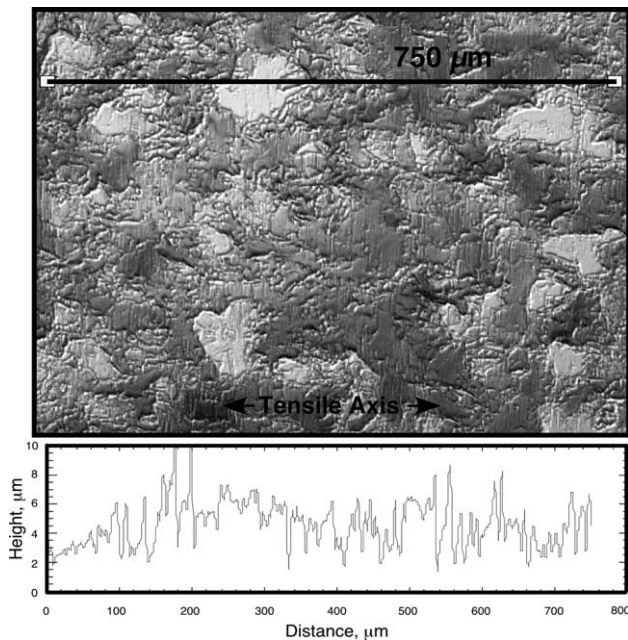
Fig. 2. A scanning laser confocal microscopy image showing the surface topography of mild steel sheet in the as-received condition and the corresponding height profile of the 750 μm trace.
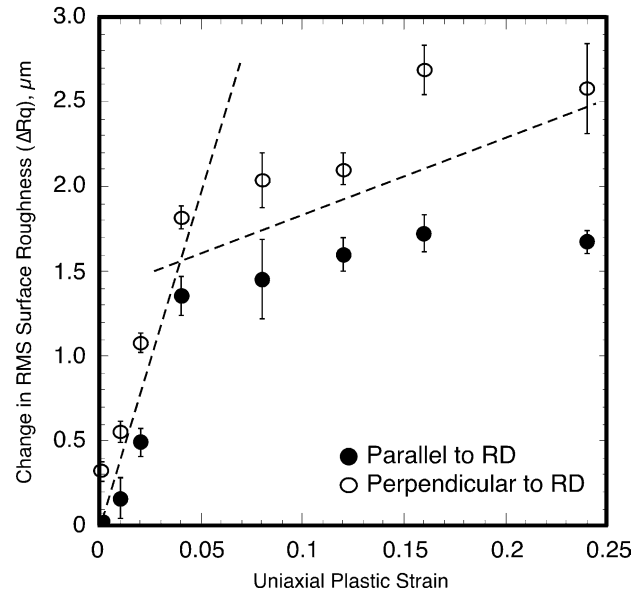
Fig. 3. The influence of uniaxial plastic strain on the surface roughening behavior of mild steel sheet as exhibited by the corrected rms roughness parameter, ΔR_q.

in surface character that are produced by the deformed surface layer [33]. For this reason, the roughness data were corrected for the initial roughness by subtracting the mean value of the initial roughness from all the subsequent roughness measurements and those corrected values are denoted by the "Δ" preceding the R_q parameter. The presence of the initial roughness had no apparent influence on the overall trends after correction; however, the magnitudes of the roughness data do not directly represent the absolute changes in the surface roughness. Note the error bars in Fig. 3 correspond to the statistical uncertainty and not to the measurement error in the roughness data. The measurement uncertainty was also corrected and the procedure used for the propagation of error in these calculations is given in [34].

The slope of the ΔR_q versus strain relationship shown in Fig. 3 defines the roughening rate for the 1010 steel under the aforementioned uniaxial loading conditions (i.e., the rate of change in the relative heights of the features on the surface as a function of plastic strain). The change in roughening rate exhibited at 4% strain in Fig. 3 is not consistent with the monotonic roughening behavior reported in the literature. However, it is important to note the following about the literature accounts: They were typically acquired from polished surfaces and, therefore, do not generally account for the influences that variations in surface hardness and grain shape have on the roughening behavior [33]. They were also largely obtained with contact profilometry, which as noted earlier, may not have insufficient measurement sensitivity to resolve the small-scale surface features.

Thus, the atypical roughening rate behavior exhibited in Fig. 3 was attributed to a combination of enhanced measurement resolution and the influence of an initial roughness. Considering the substantial impact that measurement or interpretative errors may have on the results, the deviation from the behavior reported in the literature does raise an important question: How well does a simple analysis that is based on multiple linear profile measurements and the R_q parameter represent the stochastic process, or processes, that generates a surface topography? As noted earlier, the fundamental postulate in the interpretation of any roughness measurement is that the surface profile represents the intrinsic character of the overall surface. For this reason, the validity of this postulate becomes the central issue in the answer to this question. If it is valid, it then becomes meaningful to characterize the data in a roughness profile with random process statistics.

Most statistical characterizations of surface roughness utilize time series analysis methods to some degree. These characterizations tacitly assume that the distribution of the height profile is both Gaussian and stationary. While this may enable a more straightforward statistical analysis, the literature does not provide any foundation to support such an assumption. In fact, the literature clearly shows that the appropriate statistical tools are determined by the character of the surface [35]. The form of the surface can usually be determined with a simple classification scheme such as the one put forth by Nayak [36]. That is, establish whether the surface is stationary (i.e., homogeneous), random, isotropic, etc. The surfaces of the 1010 steel were classified through a rigorous, systematic statistical evaluation thereby minimizing any uncertainty that could arise from an inappropriate assumption or from an inappropriate analytical method.

3.3. Classification of surface form

3.3.1. Assessment of Gaussian behavior

The accounts of roughening behavior in the literature place great emphasis on the significance of the changes exhibited by the R_q parameter; however, the properties of the assumed Gaussian form upon which it is based are rarely assessed [37]. Given the large number of data points contained in each profile in this evaluation, the Gaussian behavior could be straightforwardly assessed by fitting the data to the normal distribution function and analyzing the measured probability density of the profile heights [38]:

$$p(z) = \frac{1}{\sqrt{2\pi}\sigma} \exp\left(-(1/2)\left[\frac{(z-\mu)}{\sigma}\right]^2\right). \quad (3)$$

In this equation, p is the probability density of realizing a particular height (z), z is the magnitude of the height at a location along the profile length, and μ and σ are the mean and standard deviation of all the height values in the profile, respectively. Fig. 4 shows the probability density function (PDF) distributions as a function of plastic strain level in the uniaxial strain condition. The PDF data were adjusted so that the maximum probability density was zero at the mean value (i.e., the peak of the bell curves). The Gaussian analysis in the perpendicular orientation exhibits the greatest magnitudes in the numerical results from the two orientations and they are presented in Table 2. Each value shown is the mean value and the associated statistical uncertainty (UNC) of the five individual measurements performed at that strain level.

The quality of the fit to a Gaussian distribution is assessed through an analysis of the higher central moments of the distribution about the mean. The skew (third moment, σ_3) is a measure of the asymmetry of the distribution. If the distribution had an ideal Gaussian form, the skew would equal zero [38], and as shown in Table 2, the magnitude of the skew is slightly less than zero. This indicates that heights below the mean are somewhat more probable than are heights above the mean. The kurtosis (fourth moment, σ_4) is a measure of the overall shape of the distribution. An ideal Gaussian distribution has a kurtosis equal to three [38,39]. As shown, the kurtosis is slightly greater than three indicating that the curves have a slightly sharper peak and longer tails than what would occur if the distribution were ideal. Given that the surfaces were not assumed ideally Gaussian, deviations from the ideal condition are not surprising. However, the relatively
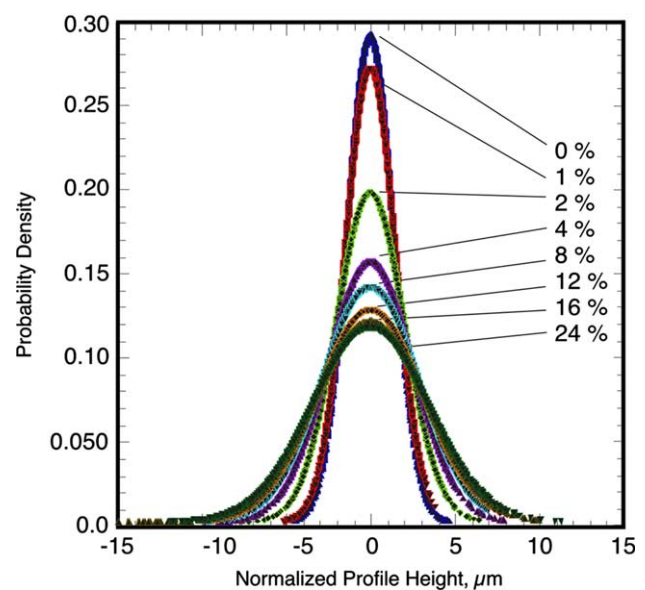
Fig. 4. Normalized probability density functions (PDF) showing the change in the surface height profile distributions as a function of uniaxial plastic strain in mild steel sheet.

Table 2
Gaussian analysis of perpendicular uniaxial strain data

Uniaxial strain	Mean, μ	Unc.	SD, σ	Unc.	Max. PDF	Unc.	Skew, σ_3	Unc.	Kurtosis, σ_4	Unc.
0.00	4.53	0.14	1.48	0.05	0.27	0.01	−0.66	0.07	3.51	0.21
0.01	12.23	0.17	1.63	0.06	0.25	0.01	−0.22	0.13	3.55	0.13
0.02	11.26	0.18	2.16	0.06	0.18	0.01	−0.20	0.13	3.50	0.27
0.04	13.39	0.56	2.90	0.06	0.14	0.01	−0.17	0.16	2.83	0.16
0.08	15.06	1.21	3.12	0.16	0.13	0.01	−0.13	0.07	2.82	0.22
0.12	14.48	0.67	3.19	0.09	0.13	0.01	−0.17	0.11	3.22	0.14
0.16	18.97	1.42	3.77	0.14	0.11	0.01	−0.08	0.15	3.48	0.14
0.24	11.90	2.96	3.65	0.26	0.12	0.02	−0.39	0.16	3.15	0.08

small magnitudes of these deviations suggest that the surfaces exhibit an overall Gaussian form [21].

The trends exhibited by the PDF curves in Fig. 4 demonstrate that the range of probable heights (i.e., the width of the distribution) increases substantially as a function of plastic strain. This is consistent with the behavior observed in the height profile data, although the change in slope at 4% strain is not apparent in this figure. Since the PDFs have been normalized, their progressive flattening does suggest a direct relationship between the magnitude of the deviation from the mean and the plastic strain. While the quality of a Gaussian fit is expected to change with the type and condition of the material of interest, these results do reveal the some general trends about a Gaussian analysis: At low levels of roughness, the probability density at the peak is quite high, resulting in short tail regions. As the roughness level increases, the probability density at the mean is considerably lower than that for the smooth surface, thereby increasing the statistical significance of the tails of the PDF.

3.3.2. Assessment of stationarity

The second key assumption regarding the general character of a surface is that it is stationary. A surface can be regarded as stationary if some statistical description of that surface is invariant with respect to a translation along the surface [36]. That is, a change in the length of a measurement does not affect the information contained within the measurement. If this condition does not hold, the statistics associated with standard time series analysis are not appropriate, and a different class of statistical tools must be employed to describe the variations in a profile [40]. As a result, establishing the degree of stationarity is essential for any substantive evaluation of surface roughness. Unlike the straightforward test for Gaussian behavior, a determination of stationarity, in the strict sense, is quite complex and cannot be verified with a simple statistical test: It requires detailed analyses of single, two-point, and multiple-point correlation functions. It should be noted that most commercial statistical software packages do not permit direct analyses of non-stationary two-point correlation functions [41].

The literature is not clear as to whether a surface can be regarded as a stationary process, or whether a roughness profile actually contains intrinsic characteristics of the surface, from which it was taken. For example, Sayles and Thomas [42] empirically demonstrated that real surface topographies cannot be treated as resulting from stationary Gaussian processes. From this, they concluded that real surfaces follow a form that corresponds to highly non-stationary Gaussian distributions. This conclusion signifies that surface roughness measurements are strongly dependent upon the actual length-scale of the measurement. It also invalidates most surface roughness studies by asserting that the measurements upon which they were based did not reflect the true character of the surfaces. In contrast, Berry and Hannay [43] argued that because Sayles and Thomas's conclusions could not be supported by the experiments they cited, Sayles and Thomas's approach has no predictive value when applied to individual topographic measurements. This contradiction exemplifies how stationary statistics cannot be assumed a priori: this property must be empirically verified.

The Weiner–Levy process [44] utilized by Sayles and Thomas can be generalized to the simple relationship between the variance and the sampling length shown in Eq. (4). This expression evaluates the validity of the stationarity assumption by comparing the surface roughness statistics from multiple measurements of different lengths.

$$\sigma_2 = L^h. \tag{4}$$

In this expression, σ_2 is the variance of the amplitudes in the profile and L is the length of the measurement. The exponent, h, indicates the degree of deviation from stationarity. That is, when $h = 0$, the variance is independent of sampling length and the statistics can be considered stationary to a first order approximation. When $h = 1$, the profile is described by Gaussian non-stationary statistics of the Weiner–Levy type.

An additional set of roughness profiles were obtained from the steel surfaces for this determination. Unlike the constant measurement length used in the previous profiles, this set of measurements incorporated a range of sampling lengths: 750, 375, 187, 93 and 46 μm. Fig.

5 is a log plot exhibiting how the variance of the amplitude distribution changed with the profile length in the 0% strain condition and in the 16% strain condition. These particular values are shown because one reflects a surface condition with a small amplitude distribution (i.e., the initial roughness) and the other reflects a surface condition with a large amplitude distribution (consisting of the initial roughness plus an additional component generated by the plastic strain), respectively. The exponent, *h*, was determined by fitting the variance data to a power law and those results are shown in Table 3. While the correlation coefficients in the 0% strain condition are slightly lower than those obtained in the 16% strain condition, the quality of the fit for both data sets is sufficient to estimate the degree of stationarity for the surfaces. The larger slope in the 16% strain condition could be an indication that the degree of stationarity decreases slightly with strain or that additional long wavelength surface features were introduced during straining.

If a roughness profile truly reflects the character of a surface, then the data contained within a single roughness profile can be used to verify the relationship between the variance and sampling length expressed in Eq. (4). That is, similar results should be obtained by dividing the length of any one profile into several equally sized segments, as the segments themselves will be representative of the overall surface. Hence, the 750-μm profiles were divided into equal segments with lengths of 375, 187, 93, 62, and 46 μm. The changes in the variance of the amplitude distribution are shown as a function of segment length for the 0% strain and 16% strain conditions in Fig. 6. As before, the exponent, *h*, was determined by fitting the variance data to a power law and those results are shown in Table 4. Note that the variance of the entire profile (i.e., 750 μm) is shown as a single data point. The correlation coefficients indicate that overall quality of the fit was relatively good and that these results were remarkably similar to those acquired from the individual measurements.

Even though the coefficients from the two analyses are comparable, the statistical approaches used to

Fig. 5. A log plot exhibiting the change in profile amplitude variance as a function of measurement length at 0% strain and at 16% strain in mild steel sheet. The slopes were used in conjunction with a generalized Weiner–Levy relationship to gauge stationarity.
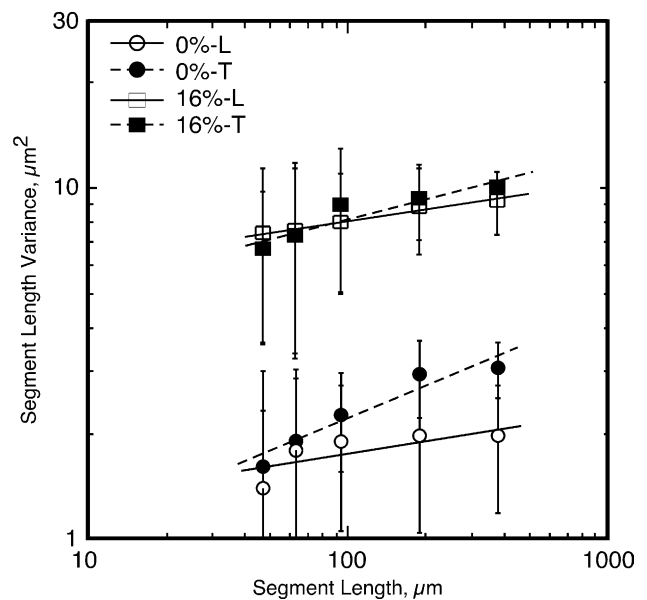
Fig. 6. A log plot exhibiting the change in segment amplitude variance as a function of measurement length at 0% strain and at 16% strain in mild steel sheet. The slopes were used to verify the stationarity.

Table 3
Measurement-based stationarity analysis results

Plastic strain level	Profile orientation	Slope	Correlation coefficient
0.00	Parallel to RD	0.154	0.863
0.00	Perpendicular to RD	0.139	0.831
0.16	Parallel to RD	0.213	0.928
0.16	Perpendicular to RD	1.961	0.939

Table 4
Segment-based stationarity analysis results

Plastic strain level	Profile orientation	Slope	Correlation coefficient
0.00	Parallel to RD	0.088	0.920
0.00	Perpendicular to RD	0.119	0.901
0.16	Parallel to RD	0.110	0.991
0.16	Perpendicular to RD	0.273	0.983

obtain them are distinctly different. Thus, the good agreement between the two data sets suggests that the generalized Weiner–Levy process approach is robust. It also indicates that the surfaces exhibit a high degree of translational invariance with respect to their statistical properties and that these properties are indeed intrinsic to the surfaces as a whole. There is a twofold significance of these results. The first is that the topography data can be generally considered as representative of the overall surface character. The second is that the location of the profile origin has no influence on any statistical interpretation of the measurement.

3.4. Spatial correlation analyses of height variations

A roughness assessment based exclusively on the mean of the amplitude distribution is not equipped to provide any information about the spatial distribution (i.e., arrangement) of the features on the surface. That is, any rearrangement in the spatial order of the profile heights will have no influence whatsoever on the magnitude of any of the roughness parameters that are derived from the PDF [45]. Thus, a different set of analytical tools must be employed to evaluate the spatial distribution. By establishing that the surfaces of the 1010 steel have both a Gaussian and, to a first order approximation, a stationary form, it can then be assumed that any distribution of heights within in a surface profile will be unaffected by a change in the position of the profile origin. This assumption provides some flexibility regarding how the arrangement of heights within a profile can be represented.

A two-point correlation function is one of the more convenient approaches to characterize spatial arrangement and it has the following general form [37]:

$$\rho(\tau) = \lim_{L \to \infty} \frac{1}{L} \int_0^L (z(x) \times z(x + \tau)) \, dx. \tag{5}$$

As shown schematically in Fig. 7, L is the sample length, $z(x)$ is the height at any point along the profile, and $z(x + \tau)$ is the height at the corresponding lag (i.e., offset) length, τ. Normalizing Eq. (5) by the variance of the roughness profile (σ_2) yields the autocorrelation function (ACF) [21]. Note that the value returned by this function for a lag of any given length is actually
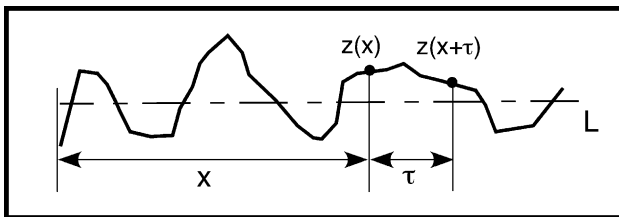
the mean of all the values evaluated over the entire roughness profile for that lag length.

Even though each profile may be considered as representative of the overall surface, the data in an individual profile are highly specific to the local region of the topography from where it was acquired. Thus, the high degree of variability between individual measurements makes an averaging approach similar to that used for the R_q analysis (i.e., a simple average of the ACF values obtained from a series of individual profiles) inappropriate to represent the correlation behavior of an entire surface. Additionally, evaluating the arrangement of heights within single roughness profiles reveals little about the correlations that may exist over the entire surface. Since a two-point correlation function is a transform of the profile data, only small variations are produced in the overall shape of the ACF for any given strain condition. For this reason, it becomes possible to average the individual values calculated for each specific lag across a series of roughness profiles taken from the same surface. In addition, averaging the large amount of data available for each ACF calculation minimizes the relative significance of any singular occurrence that may be present in any individual profile. This creates a two-point correlation function "ensemble" that describes the distribution of heights for that surface condition. Analysis of the ACF ensembles reveals any general trends that may occur in the surface topography resulting from the plastic strain. An example of this method is shown in Fig. 8 that illustrates the behavior of a typically observed ACF ensemble. The dark line in this figure is the mean ACF value determined from the five individual profiles taken at each lag in the 24% strain condition. The grey lines on either side of the solid line are the standard uncertainties (i.e., 1σ) calculated for the five values at each lag [34]. Curves similar to Fig. 8 were obtained for each strain level with roughness profiles in both the parallel and perpendicular orientations to the rolling direction. Small variations were observed in the ACF behaviors between the two orientations, but for brevity, only the results from the parallel orientation will be presented.

An autocorrelation function contains a considerable amount of information about the spatial relationships in a roughness profile. That is, when the ACF = 1, the features in the profile are defined as being perfectly correlated with themselves at that lag length. Similarly, when the ACF = 0, the features are defined as having no correlation, or completely random. The transition between the correlated and random state defines the correlation length. It is the most common characteristic derived from the ACF and it is usually assumed proportional to the decay of the ACF. One approach for estimating the correlation length is by fitting the ACF to a simple exponential and calculating the lag where the function reaches 0.1 [37]. This approach assumes

Fig. 7. A schematic diagram defining the protocol used to calculate a 2-point height correlation function.
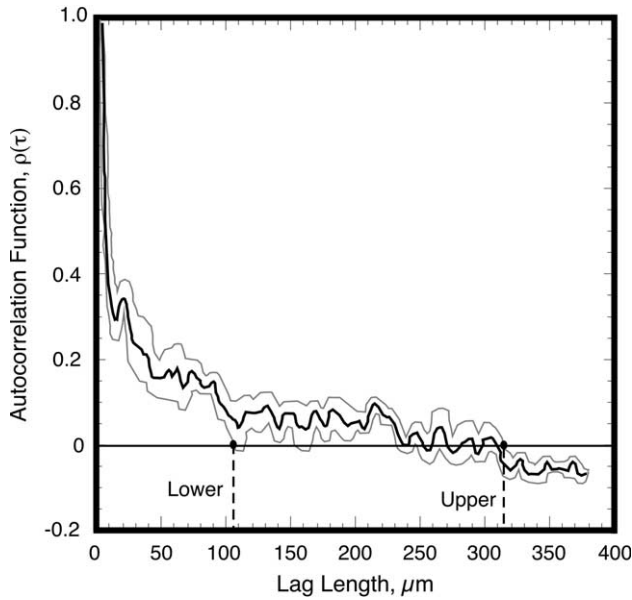
Fig. 8. The ACF ensemble in the parallel orientation to the rolling direction for mild steel sheet with 24% uniaxial plastic strain. The dark line is the mean ACF value determined from the five individual values calculated at each lag. The grey lines on either side define the uncertainty envelope associated with the five lag values.

that the ACF becomes statistically unreliable where the quality of the fit to an exponential becomes significantly degraded. Since additional analyses of long-range correlations are not practical with the data from an individual ACF, the transition from the correlated to the uncorrelated state is typically assigned to the lag where the ACF assumes a value of 0.1 (i.e., $\rho(\tau) = 0.1$). In contrast, the ACF ensemble represents the behavior of the entire surface in one direction, and not just the behavior within a single profile. Therefore, statistically significant information is likely to be present in the region of the ACF that lies between 0.1 and 0. A more general method for estimating the correlation length is required to assess the correlation of features occurring at the longer lag lengths.

Assuming this process has Markov properties, the correlation length is finite by definition. Therefore, several statistical approaches can be adopted to determine the correlation length. One of these is by integrating the ACF (Eq. (5)) from the origin to some threshold value, τ^* [46]. This is shown in the following equation:

$$CL = \int_0^{\tau^*} \rho(\tau)\, d\tau. \tag{6}$$

Since the features in the ACF are considered correlated until the ACF = 0, both the upper and lower boundaries of the uncertainty envelope (shown in Fig. 8) were integrated to the point where they first assumed a value of zero. The results of that evaluation are presented in Fig. 9A. For comparison purposes, the integration
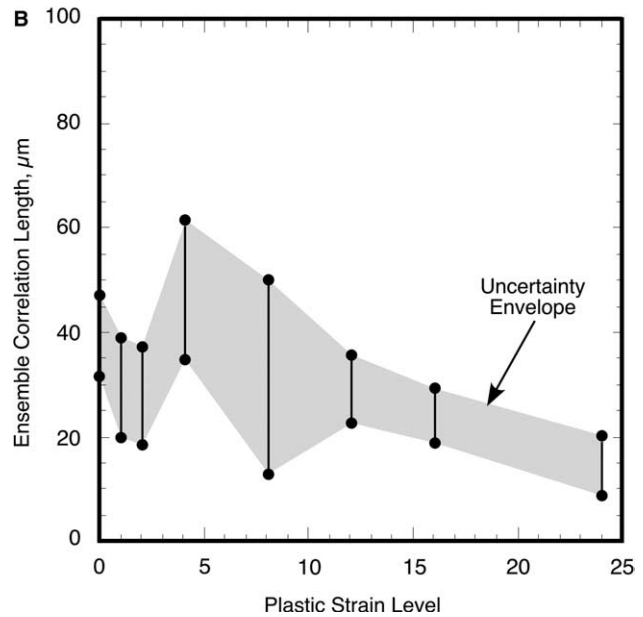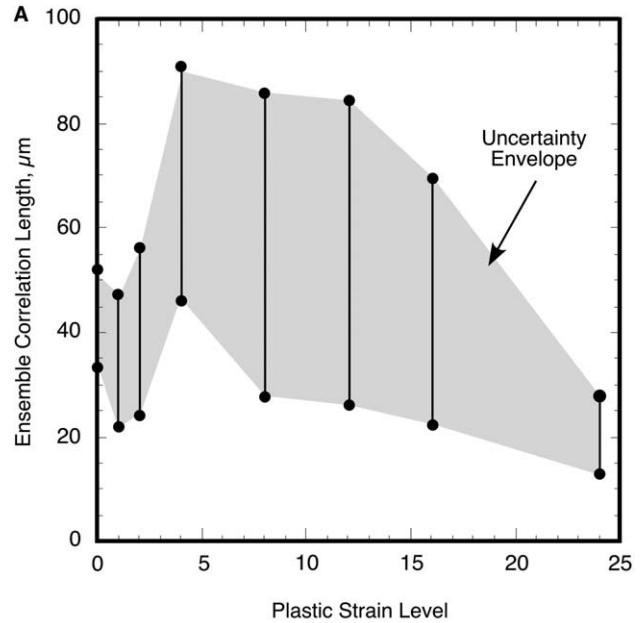
Fig. 9. The correlation lengths estimated from the ACF ensembles for mild steel sheet in the parallel orientation to the rolling direction. (A) Integrated to where the upper and lower bounds of the ACF uncertainty envelope (shown in Fig. 8) assume a value of zero. (B) The same ACF ensemble integrated to a cutoff value of 0.1.

procedure was repeated using a cutoff value of 0.1 and those results are shown as Fig. 9B. While the uncertainty envelope of the ACF is rather small, the uncertainties associated with the correlation lengths are substantially larger. This is primarily due to the discrepancies between the upper and lower lag-lengths at which the ACFs were terminated. As expected, this effect is not as significant when the function was cutoff at 0.1. However, the general shapes of the correlation length uncertainty envelopes are similar in both cases.

The results of the correlation examinations reveal two key points. The first point concerns the magnitude of the change that occurs in shape of the uncertainty envelope at approximately 4% strain for both cutoff values in Fig. 9. This is particularly interesting when compared to the R_q behavior exhibited in Fig. 3. As the slope of R_q versus strain shown in this figure reflects the roughening rate as a function of plastic strain, the change in width of the uncertainty envelope in Fig. 9 reflects the variability in the spatial distribution of the surface features as a function of plastic strain. Since the physical meanings of these two data sets are completely independent, the change in behavior that occurs at the same strain level in both figures cannot be a statistical artifact; rather, it suggests the existence of a set of common underlying physical mechanisms.

As noted earlier, plastic deformation in a polycrystalline alloy is an extremely complex process and the measurable surface roughness depends on several factors. For this reason, the resulting surface topography is an amalgam of each active mechanism during the deformation process. Additionally, each component in this deformation has a corresponding effective characteristic length scale that can be used to distinguish it. These range from the hundred-nanometer scale associated with slip steps to the several hundred-micron scale associated with slip localization.

At low levels of plastic strain, the amount of deformation that occurs within each grain depends on the individual orientation, the local Taylor factor [47], and the constraints imposed by neighboring grains at or below the surface [14]. That is, the deformation in a grain with a favorable orientation for slip will occur by primary slip in the interior regions of that grain. However, in a grain where the slip conditions are not as favorable, the deformation will tend to localize in the grain boundary regions due to the additional shear displacements required to produce grain rotation and to maintain grain-to-grain contiguity. This anisotropy produces an overall roughness character that is a mixture of both primary slip and near grain boundary deformation. Accordingly, neighboring surface grains possessing the same level of macroscopic strain can exhibit appreciably different amounts of measurable surface roughness. As the plastic strain levels and dislocation densities increase, localized work hardening makes deformation by primary slip more difficult, thereby activating additional slip systems, such as those that promote secondary slip, pencil glide and slip localization. Therefore, the common behavior exhibited at 4% strain most likely reflects a transition threshold between principal roughening mechanisms.

The second point concerns the shape of the ensemble-averaged ACF profile. It is well established in the statistical literature that if a stochastic process has stationary, Gaussian, Markov properties it is unique [48] and it must possess an ACF that decays as a simple exponential function of lag length. The fact that this profile does not exhibit such behavior specifically implies that one of these three fundamental conditions has been violated. This has significant consequences for this study as well as for all analyses of surface roughness. A violation of the stationarity condition directly disputes the validity of the fundamental postulate that serves as the basis for all surface roughness analyses: namely, that a surface profile is representative of the intrinsic character of the overall surface. If this does not hold, then a roughness profile cannot reflect any inherent property of the surface from which it was taken, thereby implying that the commonly used methods to interpret surface roughness are not meaningful. The results from the analysis of the variance with the generalized Weiner–Levy approach demonstrated that the roughness data in this study was stationary to a first order. Therefore, it can be concluded that the stationarity condition was not violated. If the stochastic process had Markov properties, then the roughness profiles must have a finite correlation length. Even though the ACF ensemble profiles exhibited long wavelength features, there is no justification for the assumption that the correlation length associated with those features diverges. Thus, the Markov condition also was not violated. Therefore, it must be concluded that the deviation from a pure exponential decay exhibited by the ensemble-averaged ACF profile is most likely related to the small deviations from Gaussian behavior present in the roughness data.

The significance of this conclusion is twofold: First, non-Gaussian behavior implies a violation of the central limit theorem of statistics [49]. That is, surface roughness profiles cannot result from linear superpositions of large numbers of statistically independent roughening events. In this case, a violation of the central limit theorem of statistics means that the deformation of a free surface must occur by a small number of statistically dominant mechanisms. This is consistent with the literature in that measurable deformation-induced surface roughness, particularly at small strain levels, is largely produced by crystallographic slip and near grain boundary deformation. Consequently, the sharp deviation in behavior exhibited at 4% strain in Fig. 3 and in Fig. 9 probably reflects a change in deformation mechanism. If so, the quality of a fit to an ideal Gaussian profile should improve above the 4% strain level. A simple test of the data shown in Table 2 revealed that the mean skew for the larger strain values (i.e., 4–24%) was approximately 0.18 as compared to approximately 0.37 for the mean skew for the smaller strains (0–2%). Similarly, the mean kurtosis was approximately 3.10 for the larger strains and approximately 3.52 for the smaller strain values. These results indicate that the divergence at 4% strain is not a statistical artifact and that it almost certainly

corresponds to an increase in the number of active deformation mechanisms. Second, the small deviations from Gaussian behavior provide direct evidence that R_q cannot completely characterize the roughening behavior of a polycrystalline material. Mean amplitude distribution parameters are all based on the presumption of ideal Gaussian behavior and, as these results demonstrate, plastically deformed surface profiles do not exhibit an ideal Gaussian form. While this presumption could hold for surfaces with more homogeneous roughening characters, such as machined surfaces, plastic deformation of a free surface appears to be too complex to be properly characterized by such a simple approach.

The results of this study demonstrate that small deviations from the ideal surface character, such as those produced by crystallographic slip, may have a pronounced influence on the accuracy of the analytical methods used to interpret the roughness data. Because of the density of data points used in this study, and the high measurement resolution provided by the SLCM technique used for the data acquisition, both the statistics associated with these small variations and the methods used to evaluate them were determined to be robust. However, additional studies are warranted to determine (a) the influence of additional roughness profiles on the width of the uncertainty envelope associated with the ACF ensemble and (b) how the individual roughening mechanisms influence surface profile statistics.

4. Conclusions

The inability to accurately predict the surface deformation morphology with numeric methods raises a serious question as to how well the analytical tools commonly used to evaluate roughness data actually represent the real surface. To address this question, roughness data were acquired from the surfaces of uniaxially strained mild steel sheet specimens with a high-resolution scanning laser confocal microscopy (SLCM) technique. A conventional plot of the rms roughness (R_q) versus plastic strain exhibited a sharp change in slope at approximately 4% strain. This change in roughening rate was determined to be inconsistent with the literature consensus of monotonic roughening behavior and it was attributed to a combination of the enhanced measurement resolution of the SLCM and an influence of the initial surface roughness.

A two-point correlation function (ACF) ensemble approach was developed to evaluate the spatial distribution of the surface features induced by the plastic strain. Integration of the uncertainty associated with the ACF ensemble to the points where the upper and lower bounds first assumed a value of zero enabled an estimation of the correlation length envelope for the ensemble. Like the plot of the rms roughness, the correlation length envelope plot also exhibited a sharp change at 4% strain. Considering that the physical meanings of the two data sets are completely independent and that plastic deformation at a free surface of a polycrystalline material is highly complex, the change in behavior at this strain level most likely represented a transition in principal roughening mechanisms.

While most roughness analyses tacitly assume that the measured surface profile conforms to stationary, Gaussian statistics, this study employed a set of rigorous analyses to establish the actual form. Small deviations from the ideal Gaussian behavior were observed in the skew and kurtosis data; however, the results indicated that a Gaussian height distribution provides a reasonably accurate characterization of the surface roughness for this material. A generalized Weiner–Levy relationship was utilized to empirically assess the degree of stationarity by evaluating the statistical variance of the roughness profile as a function of the measurement length. Even though small deviations were observed, the roughness data exhibited a high degree of translational invariance symmetry with respect to the statistical properties. From this it was determined that the surfaces were largely stationary and that the characteristics in the roughness data could be considered as representative of the surfaces as a whole.

The shape of the ACF ensemble did not exhibit a simple exponential decay, which indicated that the stochastic process responsible for surface roughening did not conform to simple stationary, Gaussian, Markov statistics. Thus, the behavior exhibited by the ACF profile implies that one or more of these three conditions was violated. A lack of stationary means that a roughness profile is not representative of the surface from which it was taken, whereas a violation of the Markov condition implies the existence of extremely long-range (i.e., exceeding several hundred microns in length) spatial correlations in these profiles. Inasmuch as a violation of either of these conditions was deemed unlikely, it was concluded that the pronounced deviation from the simple exponential form exhibited by the ACF profile was associated with the small discrepancies in the Gaussian fit. This conclusion indicated that deformation-induced surface roughness must occur by one, or just a few, statistically dominant mechanisms. This agrees with the literature which claims that deformation-induced surface roughness largely consists of near grain boundary deformation and crystallographic slip. Additional studies are warranted to determine (a) the influence of additional roughness profiles on the width of the uncertainty envelope associated with the ACF ensemble and (b) how specific roughening mechanisms influence surface profile statistics.

References

[1] Dieter GE. Mechanical metallurgy. 3rd ed. New York (NY): McGraw-Hill; 1986.

[2] Becker R. Acta Mater 1998;46(4):1385–401.

[3] Wilson WRD, Lee W. J Manuf Sci Eng 2001;123:279–83.

[4] Dai YZ, Chiang FP. J Eng Mater Technol 1992;114(Oct):432–8.

[5] Valkonen AE. Plastic deformation and roughness of free metal surfaces. Ohio State University; 1987.

[6] Abe T, Nagaki S, Akase T. Bull JSME 1985;28(236):251–8.

[7] Kienzle O, Mieztner K. Stahl Eisen 1961;81(14):950–2.

[8] Osakada K, Oyane M. Bull JSME 1971;14(68):171–7.

[9] Guangnan C, Huan S, Shiguang H, Baudelet B. Mater Sci Eng A 1990;128:33–8.

[10] Bishop JFW, Hill R. Philos Mag 1951;42(327):414–27.

[11] Kocks UF. Metall Trans 1970;1:1121–43.

[12] Hansen N. Metall Mater Trans A 1985;16:2167–90.

[13] Armstrong RW. In: Baker TN, editor. Yield, flow and fracture of polycrystals. London: Applied Science Publishers; 1983. p. 1–31.

[14] Stoudt MR, Ricker RE. Metall Mater Trans A 2002;33: 2883–9.

[15] Beaudoin AJ, Acharya A, et al. Acta Mater 2000;48:3409–23.

[16] Wu PD, Lloyd DJ. Acta Mater 2004;52:1785–98.

[17] Hurley PJ, Humphreys FJ. Acta Mater 2003;51:1087–102.

[18] Rabbe D, Sachtleber M, et al. Acta Mater 2003;51:1539–60.

[19] Thomson PF, Shafer BV. Int J Machine Tool Design Res 1982;22(4):261–4.

[20] Inagaki A, Komatsubara T, Inagaki H. Z Metallkd 1999;90(6):427–33.

[21] Thomas TR. Rough surfaces. 2nd ed. London: Imperial College Press; 1999.

[22] Radhakrishnan V. Wear 1970;16:325–35.

[23] Murthy TSR, Reddy GC. Wear 1982;83:203–14.

[24] King TG, Spedding TA. Wear 1982;83:91–108.

[25] Stoudt MR, Hubbard JB, Banovic SW. Test Meas World 2004;24(5):A7–A10.

[26] Properties and selection of metals, vol. 1, 8th ed. Metals Park (OH): ASM International; 1961.

[27] Smith WF. Structure and properties of engineering alloys. New York (NY): McGraw-Hill; 1981.

[28] VanderVoort GF. Metallography principles and practice. Materials Park (OH): ASM International; 1999.

[29] Udupa G, Singaperumal M, Sirohi RS, Kothiyal MP. Meas Sci Technol 2000;11(3):305–14.

[30] Lange DA, Jennings HM, Shah SP. J Mater Sci 1993;28(14): 3879–84.

[31] Annual Book of ASTM Standards, Section 3, Metals test methods and analytical procedures, vol. 3.01. Metals-mechanical testing; elevated and low-temperature tests; metallography. Philadelphia (PA): ASTM; 2002. p. 547–53.

[32] Metallography and microstructures, vol. 9, 9th ed. Metals Park (OH): ASM International; 1987.

[33] Stoudt MR, Banovic SW, Quarrick T. In: Baker MA, editor. 45th MWSP conference proceedings, vol. XLI. Warrendale (PA): Iron & Steel Society; 2003. p. 507–17.

[34] Taylor BN, Kuyatt CE. Guidelines for evaluating and expressing the uncertainty of nist measurement results. NIST Technical Note 1297, 1994 Edition, NIST; 1994.

[35] Longuet-Higgins MS. Philos Trans R Soc Lond A 1957;250:157–74.

[36] Nayak PR. J Lubrication Technol (Trans ASME) 1971;93: 398–407.

[37] Whitehouse DJ, Archard JF. Proc R Soc Lond A 1970;316:97–121.

[38] Walpole RE, Myers RH. Probability and statistics for engineers and scientists. New York (NY): Macmillian; 1972.

[39] Mendenhall W, Sincich T. Statistics for engineering and the sciences. 3rd ed. San Francisco (CA): Dellen; 1992.

[40] Montgomery DC, Johnson LA, Gardiner JS. Forecasting and time series analysis. 2nd ed. New York (NY): McGraw-Hill; 1990.

[41] Hanselman D, Littlefield B. Mastering Matlab 6. Upper Saddle River (NJ): Prentice-Hall; 2001.

[42] Sayles RS, Thomas TR. Nature 1978;271(2):431–4.

[43] Berry MV, Hannay JH. Nature 1978;273:573.

[44] Hsu H. Probability, random variables, & random processes. New York (NY): McGraw-Hill; 1996.

[45] Stoudt MR, Hubbard JB, Banovic SW. SAE Trans: J Mater Manuf 2005;5:50–8.

[46] Berne BJ, Pecora R. Dynamic light scattering. New York (NY): Wiley; 1976.

[47] Taylor GI. J Inst Met 1938;62:307–24.

[48] Doob JL. Ann Math 1942;43:351.

[49] Feller W. An introduction to probability theory and its applications, vol. 2. 2nd ed., New York (NY): Wiley; 1971.